Sensors & Transducers, Vol. 259, Issue 5, October 2022, pp. 19-28

www.sensorsportal.com

Sensors & Transducers

Published by IFSA Publishing, S. L., 2022
http://www.sensorsportal.com

Fibre Bragg Grating Based Optical Sensors Accuracy Improvement

[1, *] František URBAN jr., [2] Radek HELÁN and [3] František URBAN sr.

[1] Brno University of Technology, Faculty of Electrical Engineering and Communication, Dept. of Telecommunications, Technická 12, Brno, 61600, Czech Republic
[2] Network Group s.r.o., Dept. SFO, Olomoucká 91, Brno, 627 00, Czech Republic
[3] Brno University of Technology, Faculty of Electrical Engineering and Communication, Dept. of Microelectronics, Technická 10, Brno, 61600, Czech Republic
[1] Tel.: + 420736625804
E-mail: f.urban@nwg.cz

Received: 1 September 2022 /Accepted: 5 October 2022 /Published: 31 October 2022

Abstract: Fibre optic based sensors are becoming very successful tool for accurate and perturbation insensitive sensing of many non-electric and electric values. Favorite fibre sensoric structure capable of point and semi-distributed sensing of all effects influencing physical dimensions or refractive index of a fibre waveguide is the Fibre Bragg Grating. An interrogation of the grating reflectance spectrum is the important part of the fibre grating based sensorial system that can significantly affect the facilities of the measuring system and influence the applicability of the technology. The article analyses the spectrum scanning type of the grating sensor interrogation. We expose two main impacts that influence the accuracy of the measurement of the fibre grating spectral wavelength shift that bears the measured value. Both of them are connected with the quantity of the Grating Quality factor that we have defined for this purpose. The first impact refers to the way of scanning the wavelength spectrum of the sensorial grating and shows that the optimal measuring results are obtained when using the scanning filter wavelength spectrum width equal to the wavelength spectrum width of the sensorial fibre Bragg grating. The second impact lies in finding the grating design assuring the minimal size of the noise grating linewidth, also defined in this work. The work shows how the application of the specific apodization schemes to the fibre Bragg grating design can improve the noise grating linewidtg. Analysis of two suitable apodization profiles shows that the specific apodization of gratings can significantly improve the measuring accuracy of the scanning spectral interrogation of the grating based optical sensors.

Keywords: Fibre Bragg grating, Spectrum scanning, Spectrum linewidth, Apodization profile.

1. Introduction

Fibre Bragg Gratings (FBG) are the fibre longitudinal dispersive structures mostly formed as the periodical or quasi-periodical changes of the refractive index in the core of the singlemode optical fibre (SMF). The structure acts as the selective optical filter that reflects light in a narrow band of the wavelengths around the central wavelength λ_B given by

$$2\Lambda_G = s.\lambda_B/n_{eff}\ ; \quad (1)$$

where s is the integer, Braggs order; Λ_G is the Braggs period of the refractive index; n_{eff} is the effective refractive index of the waveguide with the grating.

Due to this reflection, the transmitted light lacks the part of the spectrum reflected from the grating. The reflected spectrum has the potential to be influenced by all the physical agents that can change either the

period Λ_G or the effective refractive index n_{eff} of the grating. The values that we speak of are namely temperature of the fibre, strains, bends, twists of the fibre, see Fig. 1. The induced spectrum changes can mostly be represented by the shift of the maximum of the reflexivity (minimum of the transmissivity) spectrum of the affected grating that is usually in a very accurately established relation to the measured agent.

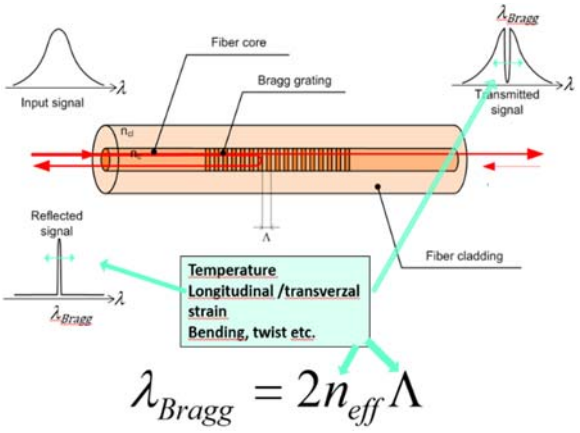

Fig. 1. Fibre Bragg Grating principle.

There is a number of methods for the evaluation of the grating spectral shift that can solve, in a compromising way, the tasks of the individual applications. One of the methods with the potential of a high resolution and a broad measuring range at the same time is the spectrum scanning.

In this way of interrogation, the source of a tuneable light is connected to the fibre isolator and then to the 50:50 symetrical coupler that sends half of the incident light power to the arm with the interrogated series of gratings and the other half of the power is sent to the arm with the reference detector. The light reflected from the FBGs is then forwarded back to the 50:50 symetrical coupler and through it to the measuring detector whose signal is then normalized using the reference detector received value. The maximum of the received power time funstion is then located and the time instant of the reception of the maximum is recalculated to the wavelength value. The structure of this interogation system is shown in the Fig. 2. In the application practice, two kinds of spectrum scanning are mostly used. The first one is based on the wavelength tuning of the narrow band optical source, often distributed feedback based laser diode (DFB), with its typical value of -20 dB drop spectral bandwidth and linewidth, $Df_{s\text{-}20} < 100$ MHz and $Dl_{s\text{-}20} \cong 0.8$ pm. The limitation of this approach is usually the tuning range and speed of the laser diode tuning. Standart telecom grade cost saving DFBs can give the modest tuning range of 10 nm in the O or C band. The second option is to scan the FBG spectrum with the light of the broadband source like superluniniscent light emiting diode (SLED) that is filtered by the tunable narrowband Fabry-Perot (FP) filter. That allows for increasing the scanning frequency to the kilohertz range and tuning range up to 100 nm, which then allows using more then 20 FBGs connected to the scanning interrogator in series. The tunable Fabry-Perot filters, however, give the one up to two orders of magnitude wider spectrum line, with the linewidth in half maximum $\Delta\lambda_{SFWHM}$ around: $\Delta\lambda_{SFWHM} \cong 60$ pm, i.e. $\Delta\lambda_{S\text{-}20} \cong \Delta\lambda_{SFWHM}/0.603 = 99.5$ pm. See Fig. 2.

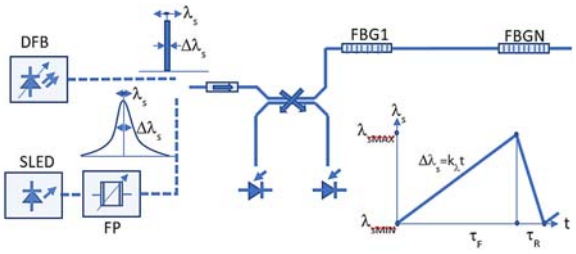

Fig. 2. Scaning interrogation scheme.

2. Spectrum Scanning and Noise

Scanning of the FBG spectrum produces the time domain photoelectric signal at the detector corresponding to the reflection spectrum of FBG. However, the time signal is not the fully linear copy of the FBG spectrum. The main peak of the time signal $I_m(t)$,

$$I_m(t) = \int_{min}^{max} Rg(\lambda).Is(\lambda - \Delta\lambda s(t)).d\lambda, \qquad (2)$$

where $\Delta\lambda_s(t) = k_\lambda.t$ is the wavelength shift of the scaning spectrum; $R_g(\lambda)$ is the spectral light reflectance of FBG; $I_s(\lambda)$ is the scanning light spectral intensity; received at the measuring detector, has its full width half maximum value different than the original FBG spectrum. It is altered by the scanning, depending on the linewidth of the scaning spectrum. The results of the scanning with the scanning spectrum FWHM equal to and wider than the FWHM linewidth of the original grating are shown in Fig. 3. The original grating design parameters of the grating represented in the Fig. 3 is L=11 mm, R_{max}= 85.6 %, $\Delta\lambda_{GFWHM}$ = 82.46 pm. Refractive index profile of this grating is the uniform sinusoid with the peak-to-peak amplitude of the modulation $\Delta n = 1.25\times10^{-4}$ and period of 450 nm superimposed to the constant level of the core refractive index of 1.468, mesured at the wavelength of 1310 nm. The graphs show that the wavelength position of the reflectance maximum stays untouched (because of the symetricity of both the grating and the scanning source spectra), but we see the change of the scanned spectra FWHM linewidths and also the change of the sharpness of the spectral maxima. That can be important for the noise influence in detecting the spectral maximum of the grating reflectance.

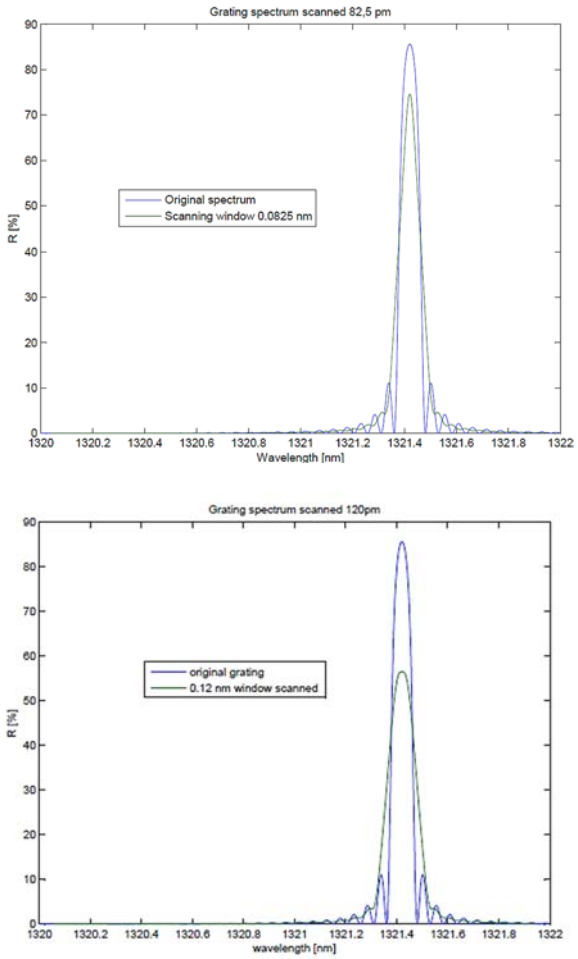

Fig. 3. Original and scanned spectrum of the uniform sinusoidal grating scanned with 82.5 pm (upper plot) and 120 pm (lower plot) scanning window.

The accuracy of the detection of the wavelength position of maximum grating reflexivity comes from the resolution of the wavelength measurement. The resolution of the wavelength measurement $\delta\lambda_G$ in this method is determined by the scanning period T_{SC}, period T_{SA} of sampling the time signal $I_m(t)$ and the scanning wavelength range λ_{Smax}-λ_{Smin}. It can be very small in case of fast sampling:

$$\delta\lambda_G=(\lambda_{Smax}-\lambda_{Smin}).\ T_{SA}\ /\ T_{SC} \leq 0.01\ \text{pm} \qquad (3)$$

The time function $I_m(t)$ is influenced by the two fundamental factors. The first one is the signal to noise ratio seen at the measuring detector circuit, the second one is the linewidth of the central maximum of the reflectance spectrum of the grating. The noise that is superimposed on the time signal of the scanned grating influences the correct determination of the position of scanned grating reflexivity spectrum. There are few sources of noise in the scanning system, detector dark current noise I_D, thermal noise of the detector load circuit I_{TH} and the detector shot noise I_{SH}. The brief analysis shows that the dominating factor here is a relatively high level of received optical signal comparing to the usual levels seen in the fiber datacommunication systems. The practical example with the typical values of the receiver bandwidth BW = 1 MHz, the transimpedance load rezistor R_C = 50 kΩ, detector dark current I_D = 1 nA, detector photoelectric current for the 100 % grating reflectance I_0 = 50 μA (corresponding to the received powers in order of 50 μW) shows the RMS values of noise currents:

$$I_D=\sqrt{(2e.I_D.BW)} = 30\ \text{pA};\ I_{TH}=\sqrt{(4k.T.BW/R_C)} = 0.57\ \text{nA};\ I_{SH}=\sqrt{(2e.I_0.BW)} = 4\ \text{nA}. \qquad (4)$$

Therefore $I_N \cong I_{SH}$ = 4 nA. Signal to noise ratio then depends on the input optical power, represented by the detector photoelectric current I_0, on grating reflectance R_{max} and on receiver bandwidth BW:

$$I_S/I_N=(I_0.\ R_{max})/\sqrt{(\ 2e.I_0.R_{max}.BW)} = = K.\sqrt{R_{max}} \cong 10^4 \qquad (5)$$

From the point of view of the grating design, we see that the important factor to minimize noise is the square root of the grating reflectance $\sqrt{R_{max}}$. Further, our application example shows that the noise root mean square I_N is in the order of 10^{-4} of the signal current at the spectral top of the grating reflexivity. The superimposed noise on the detected optical power reflexed from the scanned grating gives the origin of the rising errors in determining the time and wavelength position of the reflexing spectral maximum, see Fig. 4.

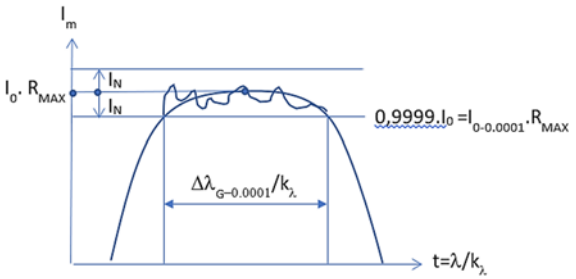

Fig. 4. Effect of superimposed noise to the location of reflectance maximum.

We can say, that the detected maximum in the current signal, composed of the light reflected from the scanned grating and superimposed noise current with the root mean square value $I_N=10^{-4}I_0$, will be most probably found in the time interval $\Delta\lambda_{G-0.0001}/k\lambda$ or in interval will be called the grating noise linewidth. It can be shown that the root mean square deviation σ of the location of detected maximum from its central position, in other words the mean error of the measurement is:

$$\sigma = \Delta\lambda_{G-0.0001}/(2.\sqrt{6}) \qquad (6)$$

The grating noise linewidth value $\Delta\lambda_{G-0.0001}$ is bound to the value of grating full width half maximum (FWHM) spectral linewidth $\Delta\lambda_{GFWHM}$. In the low reflectance uniform gratings we can work with the estimation $\Delta\lambda_{G-0.0001} \cong 0.022.\Delta\lambda_{GFWHM}$ which loses the fidelity for the cases of higher than 50 % reflectances and lower than 3 mm of lengths. Nevertheless, the next important factor in the grating design affecting the errors in the measurement of the position of maximum reflectance is the grating spectral linewidth in the half maximum $\Delta\lambda_{GFWHM}$. These two parameters, $\sqrt{R_{max}}$ and $\Delta\lambda_{GFWHM}$ are not independent in the grating design. As for that we define the grating quality factor Q_G:

$$Q_G = \sqrt{R_{max}}/\Delta\lambda_{GFWHM}; [-;\%,nm] \quad (7)$$

that depicts the suitability of the grating design for the accurate scanning interrogation, se Fig. 5. The plot here shows, that the best results in the accurate scanning interrogation of uniform gratings can be obtained for the grating lengths longer than 10 mm and the reflectance in spectral maximum around 60 %.

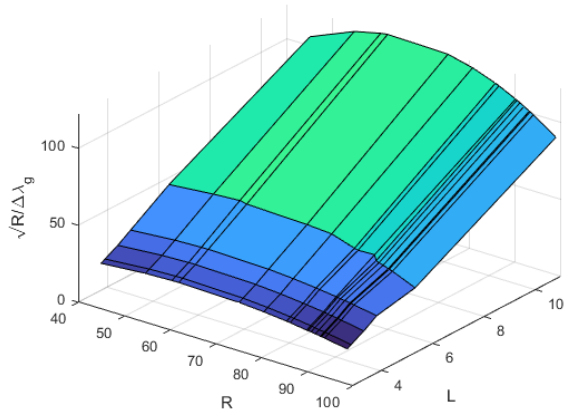

Fig. 5. Graph of the grating quality factor $Q_G = \sqrt{R_{max}}/\Delta\lambda_{GFWHM}$ on the grating reflectance R[%] and the grating length L[mm].

3. Grating Features

As we already stated, the maximum reflectance of the grating R_{max} and the reflectance spectral linewidth in the half maximum $\Delta\lambda_{GFWHM}$ of the grating are values mutually bonded. In the uniform gratings, the values of these two parameters relate to the physical length of the grating in the fibre. The graphs of Fig. 6 depict the relation of the grating half maximum linewidth $\Delta\lambda_{GFWHM}$ and the grating noise linewidth $\Delta\lambda_{G-0.0001}$to the typical lengths L of the gratings and to the reflectances R_{max}. We can see there that the value of FWHM linewidth of the uniform grating monotonically drops with increase of the grating length and with decrease of the maximal reflectance. To the contrary, the grating noise linewidth of the same uniform grating design shows the different behaviour. Whille the noise linewidth drops monotonically with the grating length, similarly like it is with FWHM linewidth, the shape of the dependence of the grating noise linewidth on the grating maximal reflectance shows the minimum close to the reflectivity of the 60%. Further, it can be seen, that the grating noise linewidth rises strongly for the grating lengths shorter than 5 mm and reflectances higher than 80 %.

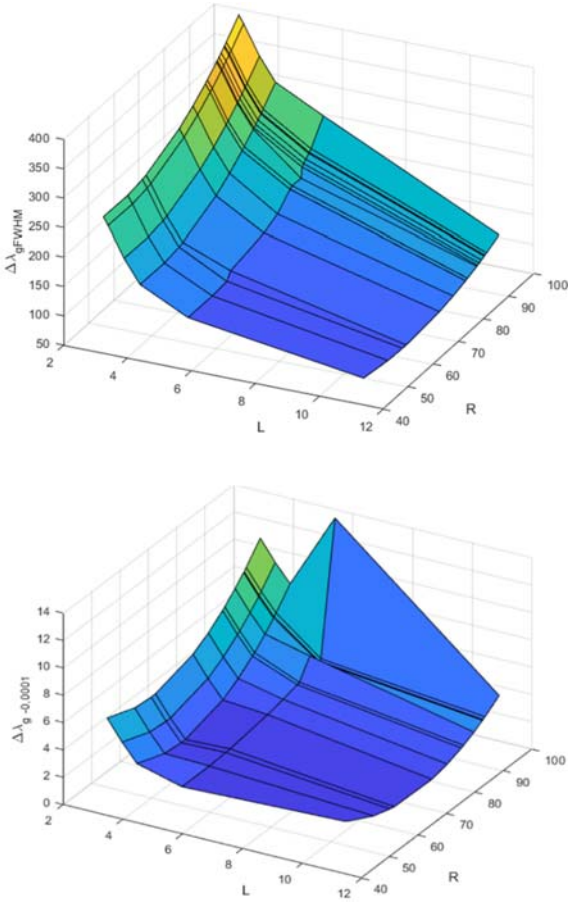

Fig. 6. Grating linewidth $\Delta\lambda_{GFWHM}$ [pm] and grating noise linewidth $\Delta\lambda_{G-0.0001}$ [pm] depending on the grating length L[mm] and the grating reflectance R[%].

When scanning the grating spectrum to locate the wavelength position of the reflectance maximum with use of an extra narowband tunable light source (DFB), $\Delta\lambda_{SFWHM} \leq 1$ pm, the time signal $I_m(t)$, eq. (2), is not distorted and linearly copies the spectral grating reflectance:

$$I_m(t) = I_{S0}.R_G(k_\lambda.t), \quad (8)$$

where I_{S0} is the photoelectric response to the light intensity of the light source; $R_G(k_\lambda.t) = R_G(\lambda)$ is the spectral reflectance of the sensorial grating.

The optimal values of the maximal grating reflectance to get the minimal noise linewidth derived

from Fig. 5 gives for the grating length L=11 mm, $R_{max} \cong$ 60.5 %. Then, for this way optimized uniform grating we get the FWHM grating linewidth $\Delta\lambda_{GFWHM}$= 63.8 pm, grating noise linewidth $\Delta\lambda_{G-0.0001}$= 1.3 pm and the mean error of establishing the wavelength of the maximum reflectance will be, according to the eq. (6), σ = 0.265 pm.

In the case of grating spectrum scanned by the tunable FP filter with the scanning spectrum FWHM linewidth similar to the spectrum linewidth of the grating itself, in spite of the shape of spectral intensity of the scanning light $I_S(\lambda)$ is similar to $R_G(\lambda)$, the linewidth and the shape of the signal $I_m(\lambda)$ is different from $R_G(\lambda)$. Analyzing this effect we find that the minimal value of the noise linewidth can be obtained when using the grating and the scanning filter with the equal value of $\Delta\lambda_{FWHM}$:

$$\Delta\lambda_{SFWHM} = \Delta\lambda_{GFWHM} \tag{9}$$

For the signal to noise ratio 10^4 we see the situation at the graph in Fig. 7, where the selected suboptimal sensual grating with L=11 mm, $R_{max} \cong$ 85.6 % and $\Delta\lambda_{GFWHM}$ = 82.46 pm gives the minimal value of scanned noise linewidth $\Delta\lambda_{GS-0,0001}$= 0.99 pm and the RMS error σ = 0.20 pm.

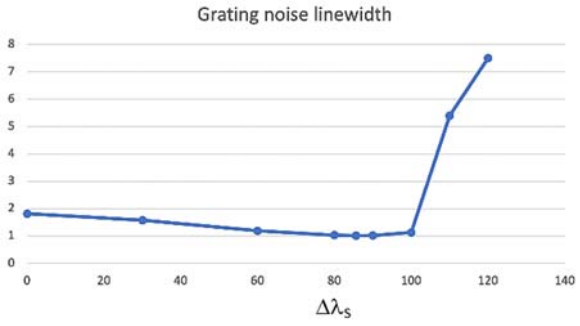

Fig. 7. Scanned noise linewidth $\Delta\lambda_{GS-0.0001}$ [pm] of the grating $\Delta\lambda_{GFWHM}$=82.5 pm scanned by the scanning spectrum FWHM linewidth $\Delta\lambda_S$ [pm].

Interesting remark can be made here, the obtained scanned noise linewidth of 0.99 pm is nearly half of the original grating noise linewidth $\Delta\lambda_{G-0.0001}$ = =1.82 pm. If the grating is scanned with the ultra narrowband tuneable source it gives the scanned noise linewidth $\Delta\lambda_{GS-0.0001}$= $\Delta\lambda_{G-0.0001}$= 1.82 pm and RMS error σ = 0.37 pm. Another feature of the scanning shows that the scanned noise linewidth rises abruptly when the sensual grating is scanned with the scanning spectrum FWHM linewidth higher that approx. 1.2 times the grating spectrum FWGM linewidth. Generalizing these findings, there are thre intervals for scanning source linewidth important from the point of the accuracy in the scanning interogation of the FBG based sensors:

$$\begin{aligned} &\Delta\lambda_{SFWHM} \ll \Delta\lambda_{GFWHM};\ \Delta\lambda_{GS-0,0001} = \Delta\lambda_{G-0.0001} \\ &\Delta\lambda_{SFWHM} \cong \Delta\lambda_{GFWHM};\ \Delta\lambda_{GS-0.0001} \cong 0.5.\ \Delta\lambda_{G-0.0001} \\ &\Delta\lambda_{SFWHM} > \Delta\lambda_{GFWHM};\ \Delta\lambda_{GS-0,0001} \gg \Delta\lambda_{G-0.0001} \end{aligned} \tag{10}$$

Progress in the grating production technology shows some other ways to further improve the accuracy of the measurement. The way lies in the modification of the grating structure by the apodization process. Simulation and the practical experiments have shown that we can decrease, by this way, the noise linewidth of the gratings noticeably below the limits achievable by the uniform gratings.

4. Apodized Gratings

Apodized grating is the grating structure where the amplitude of the periodic change of the refractive index along the fiber axis is modulated by the specific function. Well known are the apodized gratings with cos(x), $\cos^2$(x), sinc(x), Gaussian and other apodizing functions. Conventional use of the apodization is to suppress the side lobes of the grating spectrum and to increase the gradient of the sides of the main lobe of the reflectance spectrum.

Our goal with the apodization was narrowing the main peak of the grating reflectance spectrum with tolerance to the possible increase of the spectrum side lobes. We have investigated number of possible apodization schemes, but finally, we have limited the choice to the variation of cos(kx), sin(kx) and $\cos^2$(kx), $\sin^2$(kx) index amplitude apodization as these profiles showed up to be most suitable from the grating production point of view. FBG manufacturing process used for this work is based on the fibre side illumination through the grating phase mask, as seen in the Fig. 8(a). Fig. 8(b) shows the grating exposition workplace where the powerful excimer pulse UV KrF laser is used as the coherent light source, providing enough coherence length, that the two diffracted beams of +1 and -1 order generated at the phase mask can interfere and create the periodic interference pattern that spreads up to 0.5 mm below the phase mask periodically corrugated surface. This UV interference pattern is then projected to the stripped and hydrogenated fibre. Being absorbed in the fiber, the UV interference pattern maxima increase the refractive index in the core where the fiber contains small quantity of GeO_2 and H_2 as the photosensitive agents. This way the periodic refractive index variations along the fiber axis is formed. The refractive index modulation amplitude corresponds to the total UV exposition energy.

There are two principal ways to change the refractive index variations along the fiber axis and to provide the apodization for the created grating. The first one is based on the use of the intensity filter in the path of the UV beam irradiating the phase mask, as shown in the Fig. 8 a). The peak-to-peak refractive index variation induced in the fibre core exposed to the UV interference pattern under the phase mask is

proportional to the local intensity of the UV field above the phase mask and therefore proportional to the local transparency of the intensity filter. The example of the resulting index variation obtained by this method is called an impure apodization, see Fig. 8 c). It gives the index variation profile that keeps the amplitude of the variation according to the UV transparency of the filter but the mean value of the index variation and the effective refractive index n_{eff} of the fibre waveguide is not constant along the grating and changes also according to the filter transparency. That facility of the impure apodization leads to the effect of grating sections detuning and the grating partially behaves like the chirped grating. That method proved to give unsatisfactory results for our goal.

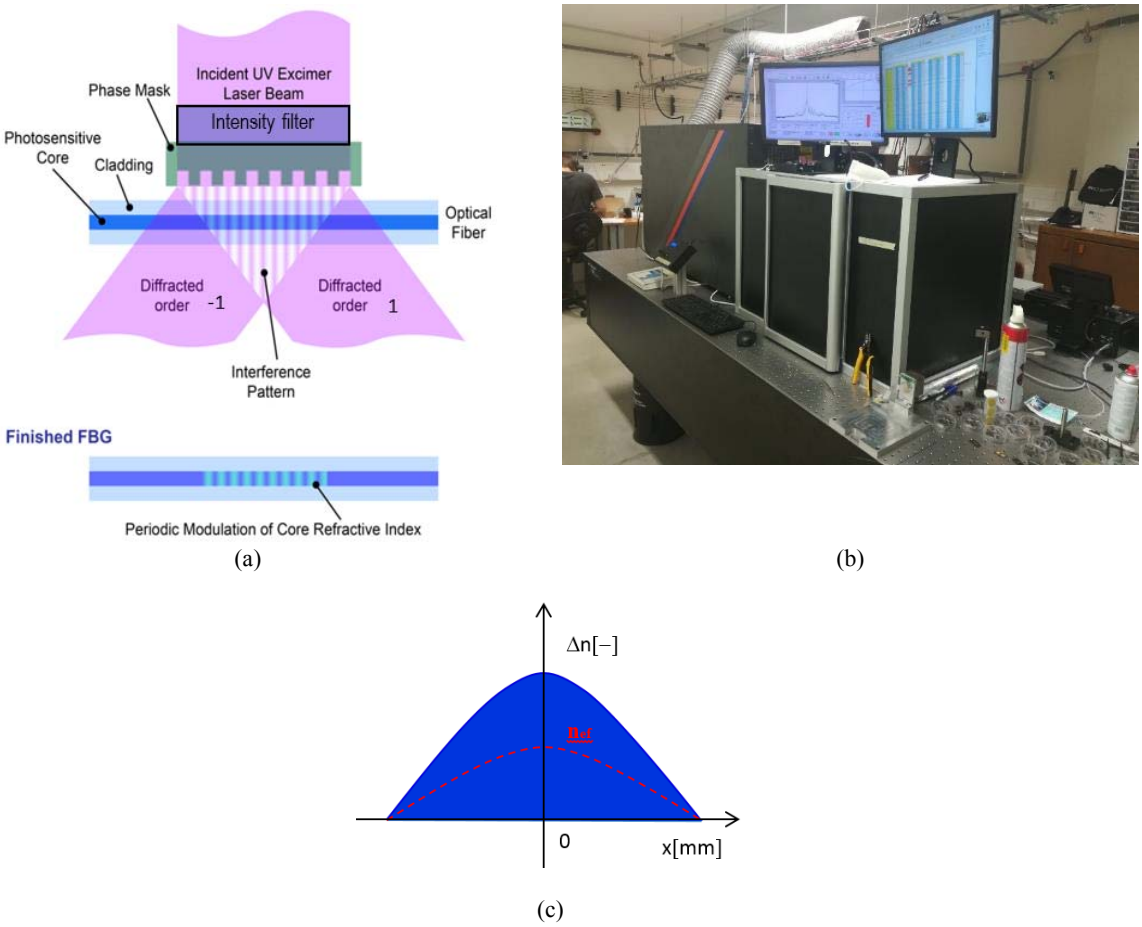

Fig. 8. a) Fibre side illumination through the grating phase mask; b) Grating exposition workplace; c) An example of index variation in the impure apodization.

The second option is to get the apodization profile by use of multiple exposition of the same interference pattern to the stretched and shifted fibre. The exposition setup is schematically shown in the Fig. 9. Here, after the first exposition of the grating component, the exposed fibre is stretched and axially shifted from its original position and subjected to the second exposition. That second step creates so called Moare effect in the overlapping of two periodic grating with slightly different grating period. This way the third and further steps can be made. Repeatability of the production limits that approach to the maximum of three consequent exposition steps. This method allows to achieve the apodization profiles based on the index amplitude functions cos(kx), sin(kx) and $\cos^2(kx)$, $\sin^2(kx)$. An important fact here is that the obtained apodization profiles can be made in the form of pure apodization. That means, the index variations always oscilate symmetrically around the constant mean value, as shown in the examples on Fig. 10, Fig. 11 and Fig. 12. With this design, the individual grating sections along the grating are not detuned from the central wavelength and the grating reflectance spectrum of the resulting structure is not widened.

Most promising apodization function from the scope of achieving the narrowest main spectral reflectance peak and the noise linewidth proved to be the index variation:

$$\Delta n(x) = n_c + \Delta n_{ph}(1 + (\sin^2(A.\pi x/L)+B).\sin(2\pi x/\Lambda_G)) \quad (11)$$

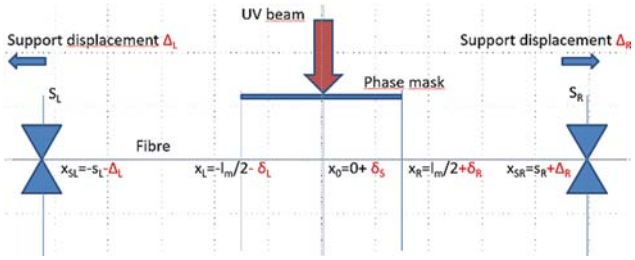

Fig. 9. Multiple exposition apodization scheme.

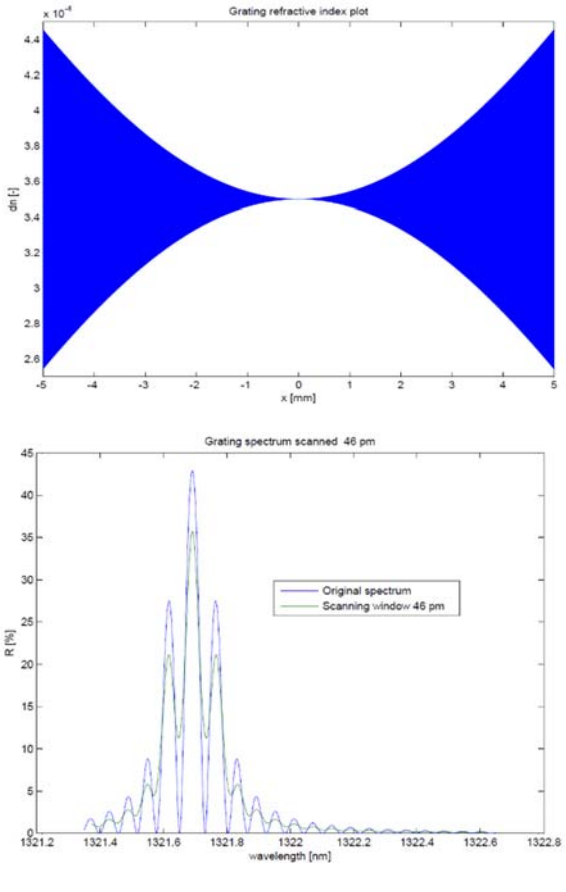

Fig. 10. Type 1 pure apodization grating design 2250-14.

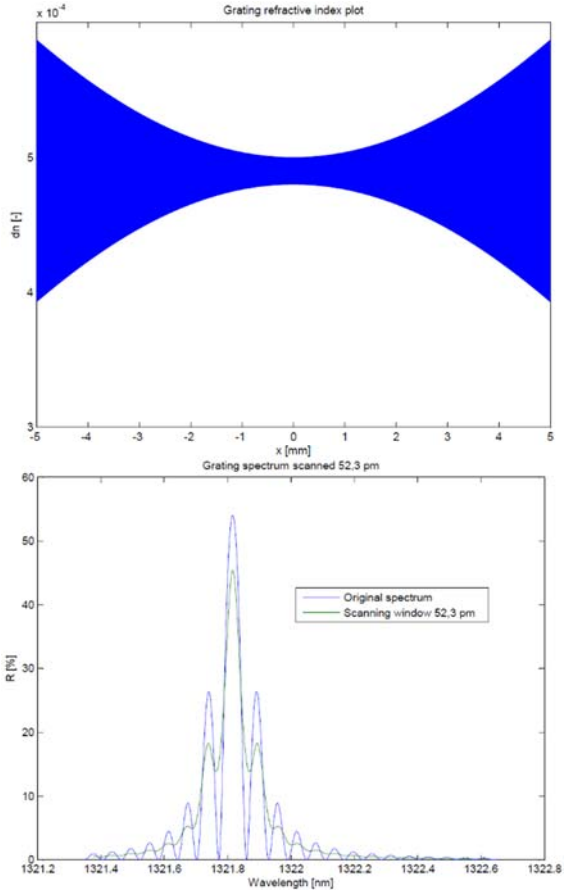

Fig. 11. Type 1 pure apodization grating design 2250-13.

The pure apodization index function from Eq. 11 can be formed by the three steps exposition process. In a complex proces of optimizing the shape coefficients Δn_{ph}, A and B, we found interesting and promissing results that have the potential for further refining. Partial results of the apodized grating design are shown in the Fig. 10 and Fig. 11. Here, both the presented gratings have the active length of 10 mm. The Fig. 10 represents the apodization grating design 2250-14 that achieved the narrowest noise linewidth of 0.912 pm, having though quite high side lobes that complicates the correct and errorless scanning process. The side lobes supression in this design is only 1.93 dB. After scanning with the optimized scanning spectrum $\Delta\lambda_{SFWHM} \cong \Delta\lambda_{GFWHM} = 46$ pm, the scanned noise linewidth is 0.495 pm and the scanned spectrum side lobe suppression 4 dB. The Fig. 11 represents the apodization grating design 2250-13 with side lobes supression (SLS) of 3.11 dB and 8.59 dB in the spectrum after the optimized scanning. That side lobe supression seems to be sufficient for reliable scannig proces. The noise linewidth achieved in this grating design is 1.05 pm which is slightly higher than in the previous design 2250-14. The scanned noise linewidth is still very good, 0.570 pm, about the half of the value for the uniform grating of the same length and reflectance.

Our second approach in using the apodization led us to the structures with the steep drop in the center of the reflectance spectrum main lobe. The apodization function that allows this feature is:

$$\Delta n(x) = \\ = n_c + \Delta n_{ph}(1 + \sin(A.\pi x/L).\sin(2\pi x/\Lambda_G)) \quad (12)$$

The representative of this design is shown at the picture in Fig. 12. The apodization profile shown there can be made by two subsequent partial expozitions with the same energy. The ($K.\Lambda_G/L$) stretch and $\Lambda_G/2$ shift has to be applied to the fibre for the second exposition. This way, two uniform gratings with equal index amplitudes, slightly different periods and the half period shift of one to the other are overlaping and creating resulting moare grating. Fig 12 shows the π - phase step in the center of the grating that is created by the superposition of the two original gratings. Analysing the reflectance spectrum of such the structure, we can observe the steep drop in the central reflectance maximum as can be seen in the Fig. 13.

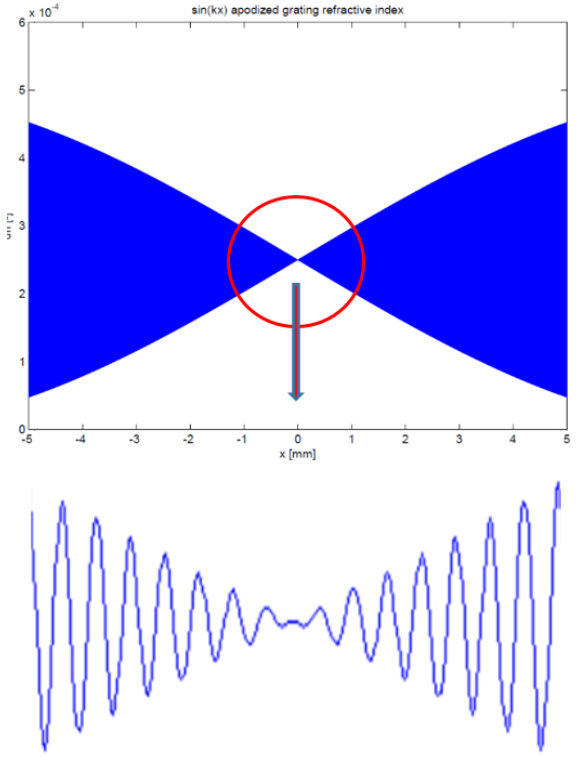

Fig. 12. Moare grating with central π -phase step.

This local reflectance minimum is very narrow and reaches the zero reflectance in the centre of the spectrum main lobe. Locating this central reflectance minimum can be therefore very accurate and the relevant noise linewidth very low. It is clearly seen that any scanning make the scanned spectrum noise linewidth only worse than the grating noise linewidth of this spectral minimum. Fig. 13 shows the original grating spectrum and scanned spectra for 50, 10 and 1 pm wide scanning spectrum. It demonstrates that the most suitable way of scanning interrogation in this case is using the ultranarrow tunable source. The scanned noise linewidth when scanned with 1 pm wide spectrum is 0,023 pm and corresponding RMS error σ = 0,005 pm, which is well below of the practically achievable scanning wavelength resolution. The results of the scanning with wider spectra are also in Table 1. Here we can see that the scanning with the spectrum linewidth wider than 10 pm rapidly deteriorates the scanned noise linewidth and measuring results. The Table 1 compares the sensorial grating features of the type 1 and type 2 apodized gratings with the uniform grating 10-60 of the same length.

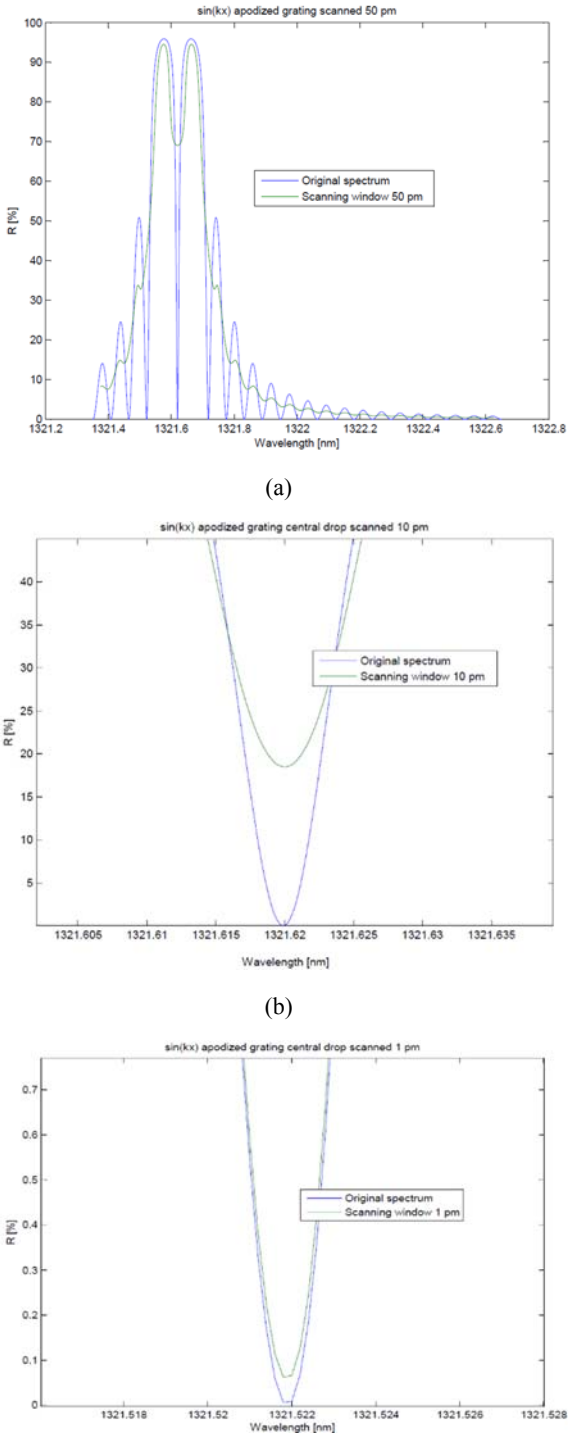

Fig. 13. Reflectance spectrum of the Moare grating and scanned spectra for a) 50 pm FWHM scanning linewidth, b) 10 pm FWHM scanning linewidth, c) 1 pm FWHM scanning linewidth.

Table 1. Comparison of uniform grating, type 1 pure apodized $\sin^2(kx)$ grating and type 2 pure apodized sin(kx) gratings.

	A	**B**	**Δn_{ph}**	**R_{max}**	**$\Delta\lambda_{GFWHM}$**	**$\Delta\lambda_{G\text{-}0.0001}$**	**$\Delta\lambda_{GS\text{-}0.0001}$ ($\Delta\lambda_{SFWHM}$)**	**σ**
	-	**-**	**x.10^{-4}**	**%**	**pm**	**pm**	**pm**	**pm**
10-60	0	1	0.8	60.5	63.8	1.3	1.125 (64 pm)	0.23
2250-13	0.28	0.1	5	54	52.35	1.05	0.570 (54 pm)	0.116
2250-14	0.35	0	3.5	43	46.0	0.912	0.495 (46 pm)	0.101
230-01	0.6	0	2.5	95.9	9.5	0.023	0.023 (1pm)	0.005
230-01	0.6	0	2.5	95.9	9.5	0.023	0.23 (10 pm)	0.046
230-01	0.6	0	2.5	95.9	9.5	0.023	3.10 (50 pm)	0.632

5. Conclusions

In this work, we have investigated the factors influencing the accuracy of the interrogation of the sensorial FBGs by scanning their spectra. The potentiality of the spectrum scanning interrogation method is the facility to achieve very fast reading of the grating reflectance spectrum maximum and so to follow even very fast changes of the measured values. Another potentiality of the method is a possible very low resolution of the measured values. To utilize that resolution, it was necessary to analyse the influence of the noise in the measurement. The analysis has showed the importance of some sensorial grating features to the measurement accuracy and errors. We have focussed the work to the evaluation of the grating spectral width and its impact to the measurement accuracy. We have found that the spectrum scanning gives the best results when the scanning spectrum width (FWHM) is equal to the spectral linewidth of the interrogated gratings. The scanning spectrum narrower than the grating spectrum linewidth gives still relatively good results with the RMS errors less than doubled with respect to the optimal scanning case. The increase of the scanning spectrum linewidth above the optimal value (equal to the grating linewidth) causes the rapid growth of the scanning noise linewidth and so the measuring errors.

The significance of the grating spectrum linewidth to the measuring errors minimization has led us to investigate the apodization of gratings, where we have found prospective ways to further increase the accuracy of the GBG interrogation without the need to increase the grating`s active length. We have found the apodization profiles $\sin^2(\pi x/L)$ and $\sin(\pi x/L)$ viable for grating fabrication and giving the encouraging results in decreasing the grating noise linewidth. Our results in this field (Figs. 10., 11., 12. and Table 1.) show that the proper design of the grating and the optimal scanning can noticeably increase the measuring accuracy and minimize the influence of the scanning process noise to the measurement. We therefore believe that the apodization of gratings has brought a novel look in the field of FBG sensing and more potential to further improvements of FBG sensor system design.

References

[1]. Luciano Mescia, Francesco Prudenzano, Advances on Optical Fiber Sensors, *Fibers,* 2, 1, 2013, pp. 1-23.

[2]. F. Sales, F. Mota, G. Guimarães, and A. Alexandria, Applications of Fiber Bragg Grating Sensors in the Industry, *International Journal of Advanced Engineering Research and Science*, 6, 2019, pp. 238-250.

[3]. J. K. Sahoa, N. Gupta, and D. Dhawan, Fiber Bragg gating sensors for monitoring of physical parameters: a comprehensive review, *Socity of Photo-Optical Instrumentation Engineers*, 59, 2020, pp. 1-35.

[4]. K. O. Hill and G. Meltz, Fiber Bragg Grating Technology Fundamentals and Overview, *Journal of Lightwave Technology*, 15, 1997, pp. 1263 - 1276.

[5]. J. M. L. Higuera, L. R. Cobo, A. Q. Incera, and A. Cobo, Fiber Optic Sensors in Structural Health Monitoring, *Journal of Lightwave Technology*, 29, 2011, pp. 587 - 608.

[6]. H. D. Lee, G. H. Kim, T. J. Eom, M. Y. Jeong, and C.-S. Kim, Linearized Wavelength Interrogation System of Fiber Bragg Grating Strain Sensor Based on Wavelength-Swept Active Mode Locking Fiber Laser, *Journal of Lightwave Technology*, 12, 33, 2015, pp. 2617 - 2622.

[7]. L. K. Cheng, W. Vliegenhart, and T. Habisreuther, Optical Fiber Grating based Technologies and Their Applications: from Nuclear Fusion to Medical, in *Proceedings of the Photonics Global Conference (PGC' 2012),* 2012, pp. 1-5.

[8]. J. P. Carvalho, Optical Sensing: Fiber Structures and Interrogation Techniques, PHD Thesis, *Universidade do Porto,* Porto, 2013.

[9]. T. K. Gangopadhyay, Prospects for Fibre Bragg Gratings and Fabry-Perot Interferometers in fibre-optic vibration sensing, *Sensors and Actuators A*, Vol. 113, Issue 1, 2004, pp. 20-38.

[10]. M. S. Ferreira, J. Bierlich, M. Becker, K. Schuster, J. L. Santos, and O. Frazão, Ultra-High Sensitive

Strain Sensor Based on Post-Processed Optical Fiber Bragg Grating, *Fibers*, pp. 142 - 149, 2014.
[11]. F. Urban jr, R. Helan, F. Urban sr., Sensoric Fiber Bragg Grating design for scanning interrogation in *Proceedings of the 8th International Conference on Sensors and Electronic Instrumental Advances (SEIA' 2022)*, Corfu, Greece, 2022, pp. 38-44.

Published by International Frequency Sensor Association (IFSA) Publishing, S. L., 2022 (http://www.sensorsportal.com).